Wenle Weng, James D. Anstie, and Andre N. Luiten

**Refractometry with ultralow detection limit using anisotropic whispering-gallery-mode resonators**

Physical Review Applied, 2015; 3(4):044015-1-044015-6

# Refractometry with Ultralow Detection Limit Using Anisotropic Whispering-Gallery-Mode Resonators

Wenle Weng,* James D. Anstie, and Andre N. Luiten

*Institute for Photonics and Advanced Sensing and School of Chemistry and Physics, University of Adelaide, South Australia 5005, Australia*

*School of Physics, University of Western Australia, Western Australia 6009, Australia*

(Received 25 January 2015; published 24 April 2015)

The intrinsic sensitivity of whispering-gallery-mode resonators aimed at measuring refractive index can be extremely high, although their practical performance is compromised by temperature fluctuations that masquerade as refractive-index changes. We present a triple-mode approach that delivers simultaneous and independent sensing of temperature and refractive-index changes in the same resonator. The frequency difference between two orthogonally polarized modes is used to sense temperature which is then actively stabilized to $\sim 1\ \mu$K over 15 minutes. We then detect a frequency difference between two modes of different wavelengths to obtain a refractive-index measurement that is free of temperature fluctuations. This triple-mode technique delivers a state-of-the-art detection limit of $8 \times 10^{-9}$ refractive-index units, despite the resonator size being 100 times larger than that typically used for sensitive refractometric sensing.

DOI: 10.1103/PhysRevApplied.3.044015

## I. INTRODUCTION

Whispering-gallery-mode resonators (WGMR) are frequently used for refractometry and reactive biosensing due to their superb intrinsic sensitivity [1–6]. Although many different sensing schemes have been developed for different scenarios, the basic principle is always the same: the sensing target, whether gas, fluid, biomolecules, or nanoparticles, interacts with the evanescent electromagnetic field near the surface of the resonator. This interaction modifies the effective optical path length for a resonant mode, thereby shifting the mode resonance frequency. The detection limit of this approach is determined by two key factors: the coupling strength of the target into the resonant mode and the minimum detectable change in mode frequency. This minimum-detectable-frequency change is usually set for passive detection schemes by photon shot noise in the frequency locking system [7–9], or by thermomechanical or thermorefractive noise in the resonator [10,11]. Active detection schemes have limits set through Schawlow-Townes processes [12,13]. One can calculate an outstanding potential refractometry sensitivity for WGMRs, although, in practice, these fundamental limits are rarely achieved because of the confounding effect of temperature fluctuations in the resonator [1,2,14,15].

In recognition of this challenge, some beautiful work has shown how to automatically reject the effect of temperature by measuring frequency differences between two orthogonally polarized modes [16]. Unfortunately, this approach is not applicable to anisotropic resonators that possess some unique and useful advantages: first, resonators made from $MgF_2$ (which is anisotropic) have substantially enhanced sensitivity for aqueous sensing [17] and thus are highly desirable for many applications. Moreover, in an anisotropic resonator, it is possible to tune the frequency difference between orthogonal modes to a convenient value using temperature tuning: for the isotropic resonator, this difference is fixed by the geometry. This problem is exacerbated for the desirable, small, and highly sensitive resonators with their large free-spectral range.

In this work, we develop an idea for temperature-free refractometry in anisotropic resonators. First, the frequency difference between two orthogonally polarized modes in the same mode family detects the resonator temperature [18–20]. In a second step, we stabilize the resonator temperature by adjusting the optical input power to the resonator so that this frequency difference is kept constant. In the third step, we compare the frequency of one of these two original modes to a third mode that has a wavelength almost exactly half that of the two former modes. The evanescent coupling of this third mode differs substantially from either of the other two modes which means that this second frequency difference is sensitive to the refractive index of the surrounding material. As we show below, there is a strong suppression of temperature-mitigated influences in this second mode difference, allowing achievement of a practical detection limit that is comparable to the best refractive-index measurement yet made with a WGMR. This detection limit is in spite of the use of a relatively large resonator (millimeter scale), which reduces the intrinsic refractometric sensitivity by a factor of $\sim 100$ over resonators more typically used in these applications (10–100 $\mu$m).

*wlweng@physics.uwa.edu.au

 

Nonetheless, the technique we propose here is equally applicable to smaller resonators, providing a path to upgrade the performance of this entire class of resonators into this new regime.

## II. EXPERIMENTS AND RESULTS

Figure 1 shows the experimental setup based around a 5-mm-radius $MgF_2$ WGMR. The output beam of a 1064-nm Nd:YAG laser is split into two beams: one passes through an acousto-optic modulator (AOM) to control the beam intensity, while the second is frequency shifted by $f_a \approx 160$ MHz in a double pass through an AOM and is used to control the frequency of this second beam. The second-harmonic output of the laser (at 532 nm) is made to double pass a third AOM, which gives a frequency shift $f_b$ of approximately 150 MHz. The three beams are then transferred by polarization-maintaining fibers into a thermal and acoustical shelter where the WGMR is mounted. The three beams are then combined by a polarization beam splitter and a dichroic filter and launched into a carefully positioned high-refractive-index prism so as to couple to modes in the resonator through frustrated total internal reflection. The frequency of all three signals is adjusted until they couple into three first-order modes with a $Q > 1 \times 10^8$. Due to the difference in the evanescent scale lengths of the three modes, the two 1064-nm modes are overcoupled while the 532-nm mode is undercoupled under operating conditions. For ease of description below, we denote the frequency of the 1064-nm transverse-magnetic (TM) mode as $f_{\mathrm{TM}}$, the 1064-nm transverse-electric (TE) mode as frequency $f_{\mathrm{TE}}$, while the frequency of the 532-nm TM mode is denoted $f_G$. The transmitted beams are separated by another polarization beam splitter and dichroic filter and registered on three photodetectors.

Figure 2 shows the resonance spectra of the three modes. The translation stage used to control the coupling distance is temperature stabilized with a thermistor-heater pair so the distance instabilities on time scale of 10–20 min do not cause observable fluctuations of the coupling.

The laser frequency is modulated at 1.638 MHz to implement the Pound-Drever-Hall (PDH) frequency-control approach that is then used to provide steering

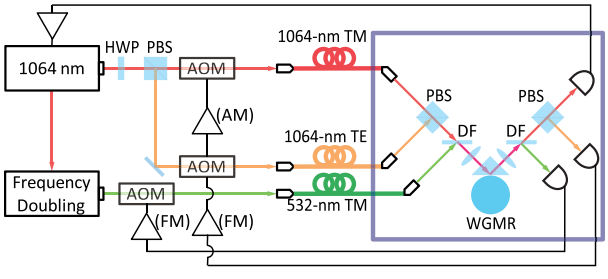


FIG. 1. Experimental setup. HWP, half-wave plate; PBS, polarization beam splitter; DF, dichroic filter; FM, frequency modulation; and AM, amplitude modulation.

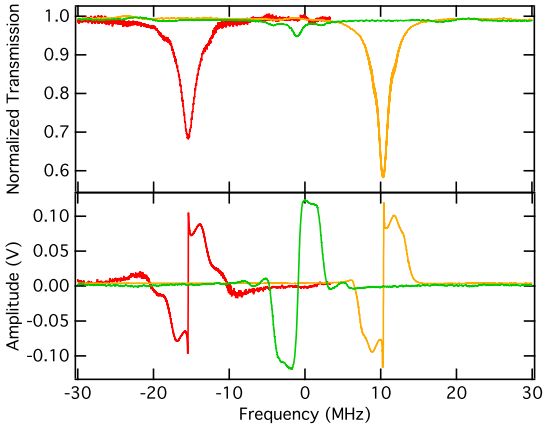


FIG. 2. Resonance spectra of the three modes in the experiment (upper panel) and their corresponding PDH error signals (lower panel). Red, orange, and green traces represent the 1064-nm TM mode, 1064-nm TE mode, and 532-nm TM mode, respectively. The PDH error signals of different modes are adjusted to the same amplitude level with electronic amplifiers.

signals for all three laser signals [21]. The error signals of the three modes are presented in the lower panel of Fig. 2 as well. The error signal of the 1064-nm TM mode is fed back to the laser frequency-modulation port, while the error signals of the other two modes are fed back to the frequency-modulation ports of the synthesizers that drove the corresponding AOMs. When all three laser signals are locked to their respective modes, we note that $f_a = f_{\mathrm{TM}} - f_{\mathrm{TE}}$ and $f_b = 2f_{\mathrm{TM}} - f_G$.

We see that $f_a$ is a proxy for the temperature of the resonator because of the different thermo-optic coefficients for ordinary and extraordinary refractive index, i.e., $1/f_{\mathrm{TM}} df_a/dT = \beta_{1064,e} - \beta_{1064,o} \equiv \beta_p$, where $\beta_{1064,o}$ and $\beta_{1064,e}$ are the thermo-optic coefficients at 1064 nm for ordinary and extraordinary light, respectively [18,19,22]. We define a new parameter $\beta_p$ as the polarization-dependent thermo-optic coefficient at 1064 nm. Furthermore, $f_b$ is also sensitive to the resonator temperature because the thermo-optic coefficient is wavelength dependent. This temperature dependence can be expressed as $1/f_{\mathrm{TM}} df_b/dT = 2(\beta_{1064,e} - \beta_{532,e}) \equiv \beta_\lambda$, where $\beta_{532,e}$ is the thermo-optic coefficient at 532 nm for the extraordinary refractive index and we define $\beta_\lambda$ as the wavelength-dependent thermo-optic coefficient [20].

We calculate the mode-frequency temperature sensitivity from the known linear expansion and thermo-optic coefficient for $MgF_2$ ($\alpha = 9.3 \times 10^{-6}$ [19], $\beta_{1064,e} = 0.25 \times 10^{-6}$, and $\beta_{1064,o} = 0.65 \times 10^{-6}$ [23]) and these are shown in Table I. We expect these estimates to be accurate to a few percent, based on the known errors in the tabulated values. We can also use the theory presented in Ref. [23] to calculate expected values for $\beta_\lambda$ and $\beta_p$ (see Table I).

For confirming the predicted values, we measure $f_b$ and $f_{\mathrm{TM}}$ as the temperature of the resonator is intentionally varied and this measurement is shown in Fig. 3.

TABLE I. Theoretical and experimental values of temperature-dependent parameters.

| Parameter | Theory | Experiment |
|---|---|---|
| $df_{\mathrm{TM}}/dT$ | −2.69 GHz/K | −2.62 GHz/K |
| $df_{\mathrm{TE}}/dT$ | −2.81 GHz/K | −2.90 GHz/K |
| $\beta_\lambda = (1/f_{\mathrm{TM}})(df_b/dT)$ | $-5.32 \times 10^{-7}$ K$^{-1}$ | $-4.77 \times 10^{-7}$ K$^{-1}$ |
| $\beta_p = (1/f_{\mathrm{TM}})(df_a/dT)$ | $-4.02 \times 10^{-7}$ K$^{-1}$ | $-5.13 \times 10^{-7}$ K$^{-1}$ |

The measurement of $f_b$ is performed with a conventional frequency counter, while $f_{\mathrm{TM}}$ is measured by comparison to a mode of a highly stabilized frequency comb. We see a strong linear relation between the two parameters, with $df_{\mathrm{TM}}/df_b = 20.00 \pm 0.02$. By combining this relation with the value of $df_{\mathrm{TM}}/dT$ in Table I, we calculate $\beta_\lambda = -4.77 \times 10^{-7}$ K$^{-1}$ in reasonable agreement with the predicted value. We then experimentally measure the relation between $f_a$ and $f_b$ as the temperature is varied (see Fig. 4). This measurement tests our expectation of a strong correlation between those parameters along with extracting a value for $\beta_p$. The linear relation shows a slope of $\beta_\lambda/\beta_p = 0.93$, allowing an estimate for $\beta_p$ (see Table I). The inset of Fig. 4 shows the residual fluctuations in $f_b$ after removing the linear slope showing deviations at the few-kilohertz level associated with slow drifts over a 10-min time scale. We note a ∼20% discrepancy between the theoretical and experimental values for $\beta_\lambda$ and $\beta_p$ that probably arises from the paucity of prior data and also because these parameters are inherently more sensitive to inaccuracy in the contributing data. We see a similar discrepancy in another experiment aimed at measuring the temperature sensitivity of a TE mode at 532 nm.

We use $f_a$ to detect the resonator temperature and then arrange to hold its value fixed by actively controlling the incident power into the 1064-nm TM mode. We increase the nominal coupled power into this mode to ∼1 mW to give us sufficient range to hold the temperature fixed over many hours. This approach gives a ∼10 Hz control bandwidth with residual fluctuations in $f_a$ corresponding to just 1 $\mu$K over 15 min (see Fig. 5). One expects that $f_b$ should also show much improved stability since its fluctuations are also dominated by ambient temperature fluctuations. We confirm this expectation using two frequency counters to record $f_a$ and $f_b$ when $f_a$ is under thermal control (see Fig. 5). We see that $f_b$ shows a strong reduction with a residual temperature drift of ∼2.5 $\mu$K/min (or ∼300 Hz/min).

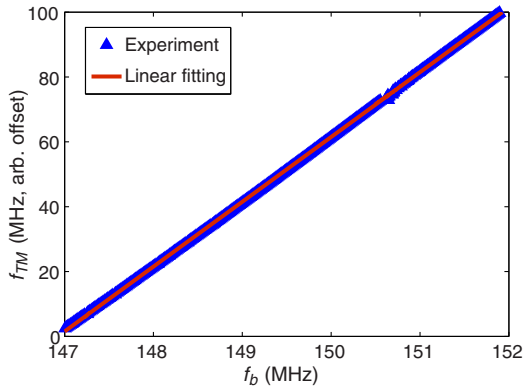


FIG. 3. The measured relation between $f_{\mathrm{TM}}$ and $f_b$ as the temperature of the resonator is intentionally varied over a range of ∼40 mK. The slope of the curve $\Delta f_{\mathrm{TM}}/\Delta f_b = 20.00 \pm 0.02$.

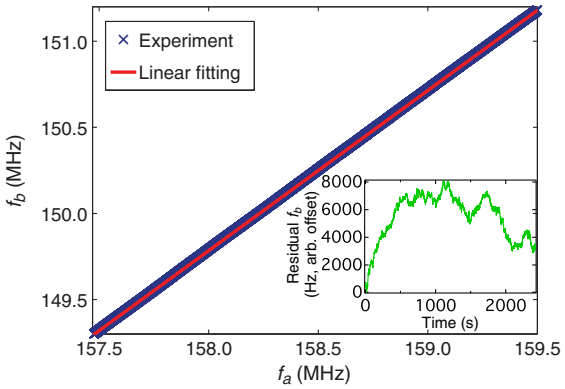


FIG. 4. The relation of $f_b$ and $f_a$ as the temperature of the resonator is intentionally varied over a range of ∼15 mK. The slope of the curve is $\Delta f_b/\Delta f_a = \beta_\lambda/\beta_p = 0.93$. The inset shows the residual $f_b$ after removal of the line of best fit.

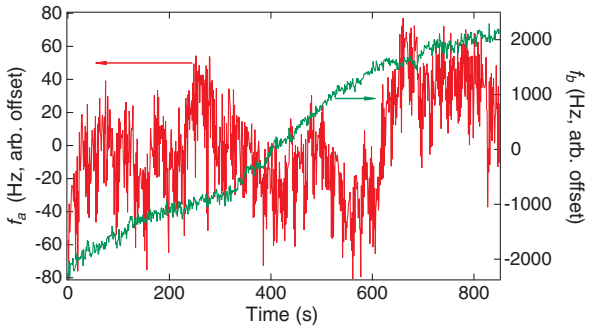


FIG. 5. Time evolutions of $f_a$ and $f_b$ over nearly 15 min when thermal control is activated. $f_a$ (red trace) is stabilized within a range of 150 Hz, while the fluctuations of $f_b$ (green trace) are ∼4 kHz.

## III. ANALYSIS OF RESULTS

Figure 6 shows the same data presented as a power spectral density (PSD), demonstrating a substantial suppression of fluctuations in both $f_a$ and $f_b$ once the control is initiated. The residual noise in $f_a$ (i.e., $f_a'$) corresponds to that expected for our temperature control system with a 5 Hz bandwidth. We note that the residual noise of $f_b$ is around a factor of 5 higher than that of $f_a$. We discuss these results in more detail following a discussion of the refractive-index sensitivity of $f_a$ and $f_b$.

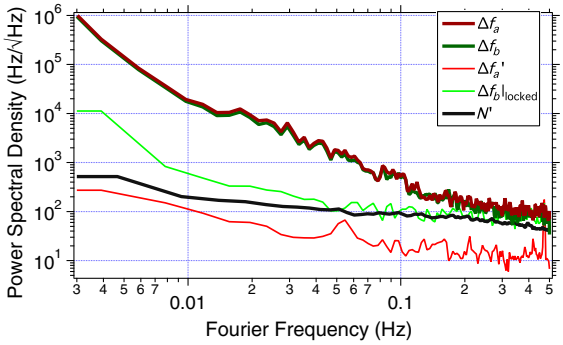


FIG. 6. The spectral density of frequency fluctuations of $f_a$ and $f_b$ when thermal control is off (thick solid lines) and activated (thin lines), respectively. When actively stabilized, the residual fluctuations of $f_b$ ($\Delta f_b|_{\text{locked}}$) are nearly 1 order of magnitude higher than the residual $f_a$ fluctuations ($\Delta f_a{}'$), limited by noise in frequency stabilization systems. The curve labeled $N'$ is the independently measured frequency stabilization noise [see Eq. (5)].

Any changes in the refractive index of the surrounding fluid or gas, or binding of biomolecules and nanoparticles to the resonator's surface, will cause a different frequency shift in all three modes because the coupling between the external environment and the mode depends both on polarization and the wavelength of the mode. In the case of a homogenous fluid of refractive index $n$ around a resonator with refractive index $n_s$, we can express the resonance frequency sensitivity as [24]

$$\frac{df}{dn} = -\frac{nc}{(n_s^2 - n^2)^{3/2}} \frac{m}{2\pi R}, \tag{1}$$

where $f$ is the resonance frequency, $c$ is the speed of light in vacuum, $R$ is the radius of the resonator, and $m$ is a polarization-dependent index, being 1 for TE mode and $2 - n^2/n_s^2$ for TM mode. This first-order expression provides the frequency sensitivity of the mode to a refractive-index change and is widely used in refractometric sensing to express the sensitivity.

However, in practice, the experimenter measures a composite frequency change, $\Delta f = (df/dn)\Delta n + (df/dT)\Delta T$, with a dependence on both resonator temperature and refractive index of the surrounding fluid. In high-$Q$ WGMR sensing applications, the temperature term in this expression commonly dominates over the refractive-index changes and thus sets the minimum detectable $\Delta n$ [14].

For our triple-mode scheme, we can express the major dependencies of $\Delta f_a$ and $\Delta f_b$ as

$$\Delta f_a = \frac{df_a}{dT}\Delta T + \left(\frac{df_{\text{TE}}}{dn} - \frac{df_{\text{TM}}}{dn}\right)\Delta n + \Gamma_a + N_a, \tag{2}$$

$$\Delta f_b = \frac{df_b}{dT}\Delta T + \left(\frac{df_G}{dn} - 2\frac{df_{\text{TM}}}{dn}\right)\Delta n + \Gamma_b + N_b, \tag{3}$$

where $\Gamma_a = f_{\text{TM}}(\gamma_{\text{TM}} - \gamma_{\text{TE}})$ and $\Gamma_b = 2f_{\text{TM}}(\gamma_{\text{TM}} - \gamma_G)$ are the relative nonlinear Kerr shifts of each mode. In calculating these Kerr shifts, care must be taken in accounting for different effective mode areas of the modes and the overlap with the total intensity distribution [20]. In our experimental situation, the intracavity power of the 1064-nm TM mode $P_{\text{TM}}$ is much higher than the other two modes and hence the overlap of this intensity distribution with the three modes determines the result, i.e., $\gamma_x = P_{\text{TM}}\kappa/n_s \int |M_{\text{TM}}|^2 |M_x|^2 dA$, where $x = \text{TE}$, TM, or $G$; $\kappa$ is the Kerr coefficient for the material; and $M_x$ is the transverse mode amplitude normalized so that $\int |M_x|^2 dA = 1$; and $dA$ is an elemental area transverse to the mode propagation direction.

We include two noise terms, $N_a = \delta f_{\text{TE}} - \delta f_{\text{TM}}$ and $N_b = \delta f_G - 2\delta f_{\text{TM}}$, in Eq. (3), which capture residual frequency fluctuations due to the finite gain of the frequency control system, where we define $\delta f_{\{\text{TE,TM},G\}}$ as the locking error for the associated mode.

We measure the resonator temperature through $f_a$ and then hold it to be constant by modulating the intracavity power of the 1064-nm TM mode $P_{\text{TM}}$, to induce temperature changes to compensate any fluctuations. We can use Eqs. (2) and (3) to obtain a value for $\Delta f_b$ in this circumstance as

$$\Delta f_b|_{\text{locked}} = \left[\frac{\beta_\lambda}{\beta_p}\left(\frac{df_{\text{TM}}}{dn} - \frac{df_{\text{TE}}}{dn}\right) + \left(\frac{df_G}{dn} - 2\frac{df_{\text{TM}}}{dn}\right)\right]\Delta n + \frac{\beta_\lambda}{\beta_p}\Delta f_a' + \Gamma_b - \frac{\alpha_b}{\alpha_a}\Gamma_a + N_b - \frac{\alpha_b}{\alpha_a}N_a, \tag{4}$$

where $\Delta f_a'$ is the residual fluctuation of $f_a$ because of the finite gain of this temperature control loop. Using the additional approximation that $(df_{\text{TM}}/dn) \approx (df_G/dn)$ from Eq. (1), we can simplify Eq. (4) to

$$\Delta f_b|_{\text{locked}} \approx -\left(\frac{df_{\text{TE}}}{dn}\Delta n + \Delta f_a'\right)\frac{\beta_\lambda}{\beta_p} + \Gamma' + N', \tag{5}$$

where $\Gamma' = f_{\text{TM}}(\gamma_{\text{TM}} + \gamma_{\text{TE}} - \gamma_G)$ is the effective Kerr noise, while $N' = \delta f_G - \delta f_{\text{TE}} - \delta f_{\text{TM}}$ is the sum of the laser locking noises.

By comparing Eq. (5) to Eqs. (2) and (3), we see that our scheme circumvents the temperature fluctuations that would otherwise set the detection noise. This expectation is confirmed in Fig. 6, which shows a 10-fold improvement in detectivity for Fourier frequencies below 0.06 Hz. Equation (5) shows that this noise immunity is achieved while the intrinsic refraction-index sensitivity is maintained at the conventional single-mode sensing level. The calculation shows that even with the large resonator used in this experiment, we obtain a detection limit of $\sim 8 \times 10^{-9}$ refractive index units (r.i.u.) in a frequency range of $10^{-1}$–$10^{0}$ Hz. This result is comparable to the best refractive-index detection limit reported so far, which

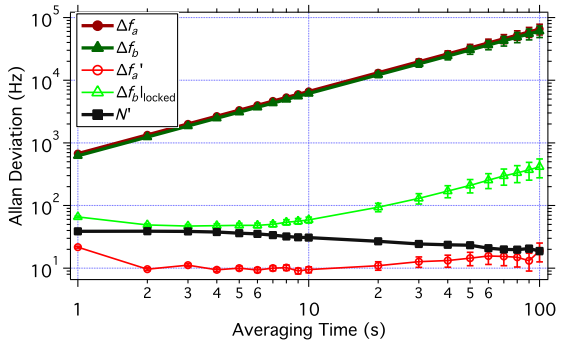


FIG. 7. Allan deviations of measured frequency instability data. The information presented with PSD in Fig. 6 is confirmed.

was achieved with a microinterferometic backscattering detection system [25].

We now address the origins of the additional fluctuations and drifts seen in $f_b$ when we thermally stabilize the resonator, based on controlling $f_a$, i.e., the difference between $f_b|_{\text{locked}}$ and $f_a'$ in Figs. 4 and 5. Equation (5) shows that the aggregate noise floors $N'$ of the frequency locking systems will appear in $f_b|_{\text{locked}}$ but not in $f_a'$. We independently measure $N'$ (see Fig. 6) and see that it is consistent with the noise seen in $f_b|_{\text{locked}}$ between 0.04 Hz and 0.5 Hz. In our experiment, this noise is mainly determined by the laser's relative intensity noise and the electronic noise of the PDH locking system. We verify that the residual locking instability due to the finite suppression gain of the feedback system is below $N'$ across the whole frequency range in this experiment.

We also consider the effect of the small disparities in mode shape and position of each of the excited modes as a potential contributor to this residual noise. However, these differences, which can be shown to be on the scale of a few microns through finite-element calculations, lead to a thermal correlation time of less than 1 ms. Thus, throughout the frequency range displayed in Fig. 6, any thermal gradients and differential temperature fluctuations arising from ambient and fundamental sources are below 10 nK and are thus negligible at the current level of performance.

Over long-time scales (more than 50 s or below 0.02 Hz), we see some low-frequency noise on $f_b|_{\text{locked}}$ (see Fig. 6) and drifts as seen in Fig. 5. One potential explanation for this is the differential Kerr effect $\Gamma'$, which contributes to $f_b|_{\text{locked}}$ as seen in Eq. (5). We expect the spectral signature of $\Gamma'$ to be identical to the free-running temperature fluctuations $f_a$, since the ambient fluctuations are mapped into $P_{\text{TM}}$, through our temperature-control technique. Earlier measurements predict that this differential Kerr effect will only contribute for Fourier frequencies below 0.01 Hz [20].

A second explanation for these low-frequency drifts arises from changes in the refractive index in the region around the resonator. The air-pressure change at the time of the experiment was ~1 hPa/h. Using the known relationship between the air pressure and the refractive index [26], we calculate an atmospheric refractive-index drift of $2.7 \times 10^{-7}$/h, causing around 60 Hz/min drift in $f_b$, in close agreement with the levels observed in Fig. 5.

We also plot in Fig. 7 the Allan deviations of the same measured frequency instability data for PSD calculations, which confirms the information presented in Fig. 6.

## IV. DISCUSSION AND CONCLUSION

Smaller resonators are generally preferable for sensing as the intrinsic sensitivity improves with the stronger evanescent field. However, our analysis shows that the triple-mode approach can deliver a detection limit comparable to the best refractometric sensors but using a resonator of millimeter size. The triple-mode approach also provides automatic suppression of the laser frequency fluctuations [27] and eliminates the need for spectra acquisition and curve fitting as required in alternative techniques [4,24].

If we were to combine this triple-mode idea with new developments in manufacturing high-$Q$ crystalline WGMRs, with a size of a few tens of microns [28], then it would be possible to obtain an extreme detection limit. We calculate that for a WGMR with a 50 $\mu$m radius, with a noise level the same as here, we would have a detection limit below $1 \times 10^{-10}$ r.i.u.. One can also foresee applications for this technique in bioparticle sensing using the high-sensitivity of $MgF_2$ WGMR in aqueous environments [17]. The reactive effect of a single bioparticle at an optimum binding location on a 1-mm-diameter $MgF_2$ WGMR [3,5] will give a signal-to-noise ratio of 1 for a single bioparticle of excess polarizability of $\sim\epsilon_0 \times 1 \times 10^{-23}$ m$^3$. This value corresponds to a bioparticle with a radius between 10 and 30 nm, indicating a detection limit that could only be achieved previously with a microresonator.

In conclusion, we present a temperature noise-suppression technique for refractometry sensing with an anisotropic high-$Q$ WGMR. The improved noise floor results in a detection limit improved by more than an order of magnitude. By combining this technique with new fabrication techniques for micron-scale crystalline microresonators, one can see a path for single-virus detection, or even single-molecule sensing.

## ACKNOWLEDGMENTS

The authors gratefully acknowledge financial support from the Australian Research Council under Grants No. DP0877938, No. FT0991631, No. LE110100054, and No. LE100100009 that enabled this work. The authors also wish to acknowledge the South Australian Government who have provided generous financial support through the Premier's Science and Research Fund. W. W. gratefully acknowledges financial support from China Scholarship Council and University of Western Australia.

[1] J. Silverstone, S. McFarlane, C. Manchee, and A. Meldrum, Ultimate resolution for refractometric sensing with whispering gallery mode microcavities, Opt. Express **20**, 8284 (2012).

[2] A. M. Armani, R. P. Kulkarni, S. E. Fraser, R. C. Flagan, and K. J. Vahala, Label-free, single-molecule detection with optical microcavities, Science **317**, 783 (2007).

[3] F. Vollmer, S. Arnold, and D. Keng, Single virus detection from the reactive shift of a whispering-gallery mode, Proc. Natl. Acad. Sci. U.S.A. **105**, 20701 (2008).

[4] J. D. Swaim, J. Knittel, and W. P. Bowen, Detection of nanoparticles with a frequency locked whispering gallery mode microresonator, Appl. Phys. Lett. **102**, 183106 (2013).

[5] F. Vollmer and L. Yang, Label-free detection with high-Q microcavities: A review of biosensing mechanisms for integrated devices, J. Nanophotonics **1**, 267 (2012).

[6] A. Schweinsberg, S. Hocdé, N. N. Lepeshkin, R. W. Boyd, C. Chase, and J. E. Fajardo, An environmental sensor based on an integrated optical whispering gallery mode disk resonator, Sens. Actuators B **123**, 727 (2007).

[7] T. Day, E. K. Gustafson, and R. L. Byer, Sub-hertz relative frequency stabilization of two-diode laser-pumped Nd:YAG lasers locked to a Fabry-Perot interferometer, IEEE J. Quantum Electron. **28**, 1106 (1992).

[8] J. Reichert, R. Holzwarth, T. Udem, and T. W. Haensch, Measuring the frequency of light with mode-locked lasers, Opt. Commun. **172**, 59 (1999).

[9] A. Schliesser, G. Anetsberger, R. Riviere, O. Arcizet, and T. Kippenberg, High-sensitivity monitoring of micromechanical vibration using optical whispering gallery mode resonators, New J. Phys. **10**, 095015 (2008).

[10] M. L. Gorodetsky and I. S. Grudinin, Fundamental thermal fluctuations in microspheres, J. Opt. Soc. Am. B **21**, 697 (2004).

[11] A. B. Matsko, A. A. Savchenkov, N. Yu, and L. Maleki, Whispering-gallery-mode resonators as frequency references. I. Fundamental limitations, J. Opt. Soc. Am. B **24**, 1324 (2007).

[12] A. L. Schawlow and C. H. Townes, Infrared and optical masers, Phys. Rev. **112**, 1940 (1958).

[13] M. Lax, Classical noise v. noise in self-sustained oscillators, Phys. Rev. **160**, 290 (1967).

[14] I. M. White and X. Fan, On the performance quantification of resonant refractive index sensors, Opt. Express **16**, 1020 (2008).

[15] J. D. Swaim, J. Knittel, and W. P. Bowen, Detection limits in whispering gallery biosensors with plasmonic enhancement, Appl. Phys. Lett. **99**, 243109 (2011).

[16] T. Le, A. Savchenkov, N. Yu, L. Maleki, and W. Steier, Optical resonant sensors: A method to reduce the effect of thermal drift, Appl. Opt. **48**, 458 (2009).

[17] F. Sedlmeir, R. Zeltner, G. Leuchs, and H. G. Schwefel, High-$Q$ $MgF_2$ whispering gallery mode resonators for refractometric sensing in aqueous environment, Opt. Express **22**, 30934 (2014).

[18] D. V. Strekalov, R. J. Thompson, L. M. Baumgartel, I. S. Grudinin, and N. Yu, Temperature measurement and stabilization in a birefringent whispering gallery mode resonator, Opt. Express **19**, 14495 (2011).

[19] I. Fescenko, J. Alnis, A. Schliesser, C. Wang, T. Kippenberg, and T. Hänsch, Dual-mode temperature compensation technique for laser stabilization to a crystalline whispering gallery mode resonator, Opt. Express **20**, 19185 (2012).

[20] W. Weng, J. D. Anstie, T. M. Stace, G. Campbell, F. N. Baynes, and A. N. Luiten, Nano-Kelvin Thermometry and Temperature Control: Beyond the Thermal Noise Limit, Phys. Rev. Lett. **112**, 160801 (2014).

[21] E. D. Black, An introduction to Pound-Drever-Hall laser frequency stabilization, Am. J. Phys. **69**, 79 (2001).

[22] A. A. Savchenkov, A. B. Matsko, V. S. Ilchenko, N. Yu, and L. Maleki, Whispering-gallery-mode resonators as frequency references. II. Stabilization, J. Opt. Soc. Am. B **24**, 2988 (2007).

[23] G. Ghosh, *Handbook of Optical Constants of Solids: Handbook of Thermo-Optic Coefficients of Optical Materials with Applications* (Academic Press, New York, 1998).

[24] I. Teraoka, S. Arnold, and F. Vollmer, Perturbation approach to resonance shifts of whispering-gallery modes in a dielectric microsphere as a probe of a surrounding medium, J. Opt. Soc. Am. B **20**, 1937 (2003).

[25] Z. Wang and D. J. Bornhop, Dual-capillary backscatter interferometry for high-sensitivity nanoliter-volume refractive index detection with density gradient compensation, Anal. Chem. **77**, 7872 (2005).

[26] A. Lewis, Ph.D. thesis, University of London, 1993.

[27] T. Lu, H. Lee, T. Chen, S. Herchak, J.-H. Kim, S. E. Fraser, R. C. Flagan, and K. Vahala, High sensitivity nanoparticle detection using optical microcavities, Proc. Natl. Acad. Sci. U.S.A. **108**, 5976 (2011).

[28] S. Okamoto, K. Inaba, T. Iida, H. Ishihara, S. Ichikawa, and M. Ashida, Fabrication of single-crystalline microspheres with high sphericity from anisotropic materials, Sci. Rep. **4** (2014).